1

Introduction to Smart Antennas

1.1 Introduction

Smart antennas, also known as intelligent antennas or adaptive arrays, are a key technology for advanced wireless systems, such as satellite communications, inter-satellite links, radars, sensors, mobile communications (5G and beyond), wireless local area networks, global navigation satellite systems, and wireless power transfer. One of the most important features of smart antennas is electronic beam scanning or switching. Smart antennas enable wireless systems to achieve optimum performance and increase channel throughput by electronically steering maximum radiation towards the desired directions while forming nulls against interfering sources.

The adaptive array is 'smart' because it has signal processing units with smart signal processing algorithms. Recent years have seen the development of efficient algorithms for direction of arrival (DOA) estimation and adaptive beamforming. Algorithms for adaptive beamforming include the classical least mean squares (LMS) type algorithm, constant modulus algorithm (CMA) etc. Traditional smart antennas are, however, complicated in structure, bulky in size, and costly. Thus, it is highly desirable to reduce the size, mass, power consumption, and cost of smart antennas.

Generally speaking, smart antennas can be divided into three components: the antenna, the beamforming network (BFN), and the signal processing unit. It is believed that radio frequency (RF) designs such as the architecture design and configurations of antenna and BFN play an important role in determining the overall cost of a smart antenna. A good example is the phased array in which each of the antenna elements has its own RF chain, and the number of active antenna elements determines the number of transmit/receive (T/R) modules and the complexity of the BFN. An active phased array with 1000 antenna elements typically requires 1000 RF phase shifters, 1000 RF transceivers, and a highly complicated BFN, resulting in large size, heavy weight, high power consumption, and high cost. For civilian applications, it is crucial to develop low-cost smart antennas. Here low-cost smart antennas refer to antenna systems which can achieve electronic beam scanning, multiple beams or electronic beam-switching, and have significantly lower cost compared to traditional smart antennas such as phased arrays or digital beamforming smart antennas. Low-cost smart antennas can be achieved by designing innovative antenna system architectures that require a

Low-cost Smart Antennas, First Edition. Qi Luo, Steven (Shichang) Gao, Wei Liu, and Chao Gu.

significantly reduced number of T/R modules and RF phase shifters, or simplified BFNs with low-cost beamforming algorithms.

This book focuses on the RF design of smart antennas from the aspect of the array antenna, BFN, and related beamforming algorithms. The main purpose of the book is to present the techniques of RF designs of low-cost smart antennas as well as the hardware implementations of the antenna and the BFN. As multiple-input multiple-output (MIMO) antennas are often regarded as one type of smart antennas, compact-size MIMO antennas are included as one special type of low-cost smart antennas in this book. Due to the importance of beamforming algorithms for smart antennas, one chapter on beamforming algorithms is also included and many examples are discussed.

This chapter will provide an introduction to the fundamental concepts of antennas, array antennas, and smart antennas, laying a foundation for the following chapters. Configurations of smart antennas are also explained and discussed.

1.2 Antenna Fundamentals

In this section, some fundamental parameters of antennas are briefly presented, including input impedance, bandwidth, radiation pattern, polarisation, efficiency, and gain. These are key parameters for an antenna and are critical for the radiation performance of smart antennas.

1.2.1 Antenna Impedance and Bandwidth

The input impedance of the antenna is defined as the ratio of voltage to current at the terminal of the antenna. It is the ratio of the voltage to current or the ratio of the appropriate components of the electric to magnetic fields at the feed point [1]. The impedance of the antenna is usually a complex number and it is frequency dependent. It can be expressed as

$$Z_A = R_A + jX_A \tag{1.1}$$

where Z_A, R_A and X_A represent the antenna impedance, antenna resistance, and antenna reactance at the terminal of the antenna, respectively. The antenna resistance includes the radiation resistance (R_r) and the loss resistance (R_L) of the antenna

$$R_A = R_r + R_L \tag{1.2}$$

The radiation resistance is related to the power radiated by the antenna, and the loss resistance is associated with the power dissipated in the antenna due to the losses from the dielectric material and conductor. For a multi-port antenna, as a result of the mutual impedance between different ports, the input impedance of the antenna becomes [2]

$$Z_{A,i} = V_i/I_i = Z_{ii} + \sum_{j \neq i} Z_{ij} I_j / I_i \tag{1.3}$$

where $Z_{A,i}$ represents the input impedance at port i, Z_{ii} is the self-impedance of the i_{th} port, Z_{ij} is the mutual impedance between ports i and j, and I represents the current at the port of the antenna. As shown in Equation 1.3, the input impedance at port i is related to the excitations from other ports through the mutual impedance. Ideally, if

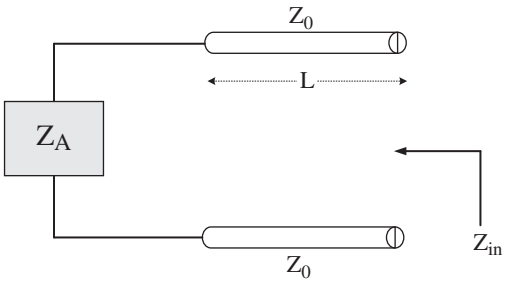

Figure 1.1 The equivalent circuit of the input impedance of the antenna with transmission line.

the mutual impedance is very small, the input impedance of each port is independent of the excitations of other ports. It is required that the antenna is impedance matched to the transmission line otherwise the antenna cannot radiate efficiently. As shown in Figure 1.1, when the antenna is terminated with a transmission with the impedance Z_0 and length L, the input impedance is

$$Z_{in} = Z_0 \frac{Z_A + jZ_0 \tan(L/\lambda)}{Z_0 + jZ_A \tan(L/\lambda)} \tag{1.4}$$

where λ is the wavelength in free space.

Figure 1.2 shows the input impedance of a typical probe-fed rectangular patch antenna. This patch has resonance at 9.75 GHz and the feeding coaxial cable has impedance of 50 Ω. This patch is printed on a 1.57 mm thick RT/Duroid 5880 substrate ($\varepsilon_r = 2.2$). As shown in Figure 1.2, at the resonance of the antenna the imaginary part of the input impedance is close to zero while the real part of the input impedance is close to 50 Ω. The reflection coefficient of the antenna is defined as

$$\Gamma = \frac{Z_{in} - Z_0}{Z_{in} + Z_0} \tag{1.5}$$

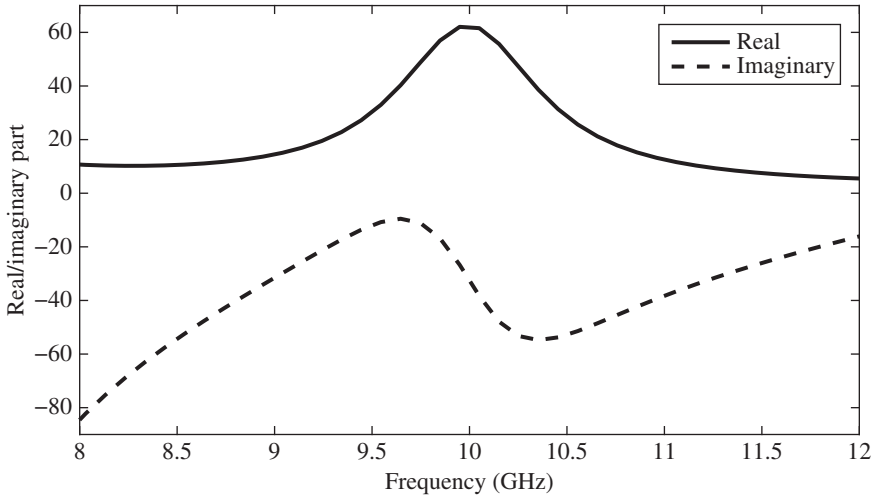

Figure 1.2 The input impedance of a typical probe-fed square patch antenna.

The concept of voltage standing wave ratio (VSWR) is introduced as a measure to show how well the antenna is matched. It is defined as the ratio of the maximum voltage (V_{max}) to the minimum voltage (V_{min}) in standing wave pattern along the transmission line. It is related to the reflection coefficient by

$$VSWR = \frac{V_{max}}{V_{min}} = \frac{1 + |\Gamma|}{1 - |\Gamma|} \tag{1.6}$$

As shown in Equation 1.6, VSWR is a real number that is always greater than or equal to 1. A VSWR of 1 indicates that there is no mismatch loss, while higher values of VSWR imply that there is large mismatch loss. Another parameter that can be used to quantise the matching of the antenna is return loss, which is defined as the ratio of rejected power against the input power to the antenna port. It is specified in decibels (dB) and is expressed as

$$RL = -20 \log |\Gamma| = -20 \log \left(\frac{VSWR - 1}{VSWR + 1} \right) \tag{1.7}$$

Another parameter that is equivalent to the return loss is the amplitude of the reflection coefficient |S11|. The |S11| represents how much power is reflected from the antenna. Generally speaking, the bandwidth of the antenna is defined as the frequency range where the return loss is larger than 10 dB ($|S11| < -10$ dB) or the VSWR is smaller than 2. In some applications, such as the mobile phone devices, the bandwidth of the antenna is defined as return loss larger than 6 dB while in base station application it is always desirable to have the return loss larger than 15 dB. Figure 1.3 shows the return loss and VSWR of the patch antenna presented in Figure 1.2. The 10 dB return loss bandwidth of the patch is approximately 5.8% at the central frequency of 9.75 GHz.

1.2.2 Radiation Patterns and Efficiency

The radiation pattern of the antenna shows the distribution of the radiated power in the far-field. It is defined as 'a mathematical function or a graphical representation of the

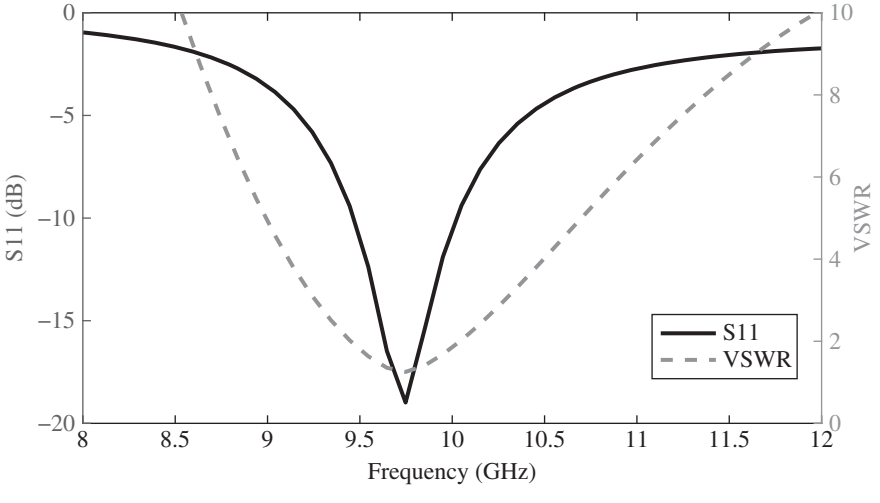

Figure 1.3 The return loss and VSWR of the patch antenna.

radiation properties of the antenna as a function of space coordinates' [1]. The power varies as a function of the angles that are observed in the far-field region of the antenna. In the far-field region, the radiation pattern does not change with distance. The far-field is defined as

$$R > \frac{2D^2}{\lambda} \tag{1.8}$$

$$R >> \lambda \tag{1.9}$$

$$R >> D \tag{1.10}$$

where D is the maximum dimension of the antenna and λ is the free space wavelength. The reactive near-field is the region that is close to the antenna. In this region, the electrical and magnetic fields are often complicated and are difficult to measure. This region is defined as

$$R < 0.62\sqrt{\frac{D^3}{\lambda}} \tag{1.11}$$

Between the far-field and reactive near-field region is the radiative near-field, which is also referred to as the Fresnel region. In this region there are no reactive field components from the antenna and the radiating fields begin to emerge. Figure 1.4 illustrates these regions of the antenna.

Figure 1.5 shows the far-field radiation patterns of some typical antennas. The directivity (D) is defined as the radiated power per unit solid angle compared to what would be received by an isotropic radiator [3]. As shown in Figure 1.5, different types of antenna have different directivity. The microstrip patch normally has a broad radiation pattern with moderate directivity. The dipole has an omnidirectional radiation pattern with typical gain of 2.3 dBi. The radiation pattern of the horn antenna has higher directivity. The directivity of the antenna can be increased by using an array antenna, as shown in Figure 1.5d.

The half-power beamwidth (HPBW) of an antenna is an important parameter for many applications, such as the base station antenna. It shows the angular range where

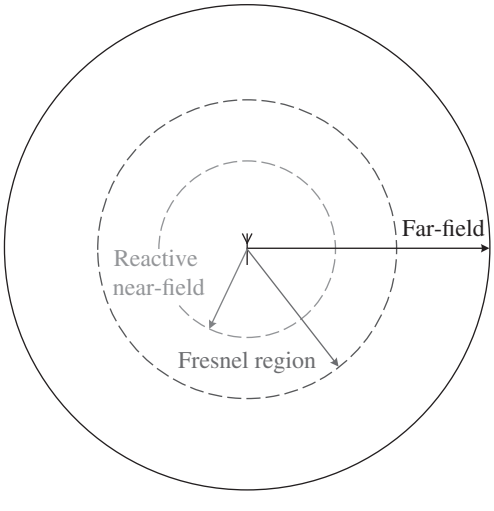

Figure 1.4 The different regions of the antenna field.

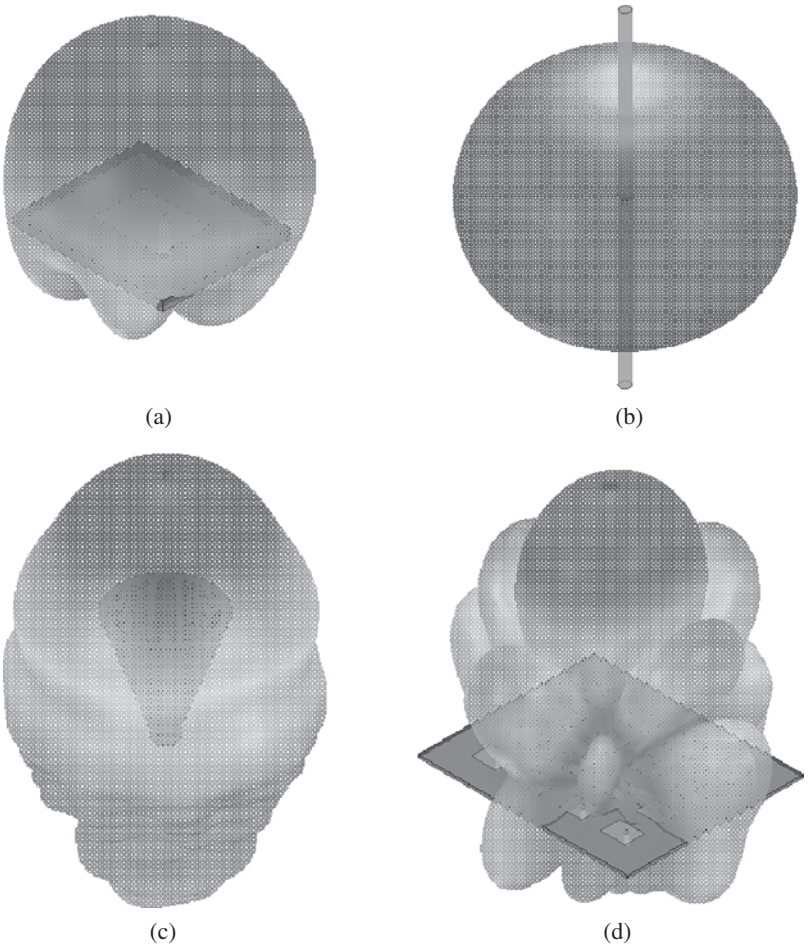

Figure 1.5 The radiation patterns of some typical antennas: (a) microstrip patch, (b) dipole antenna, (c) circular horn, and (d) microstrip array.

the radiated power has dropped by 50%. When plotting the radiation pattern in dB scale, the HPBW is where the power is reduced by 3 dB. Figure 1.6 shows an example of a directional radiation pattern that is plotted as the radiated power in dB versus the elevation angle (θ). High-directivity antennas always have a narrow HPBW, which can be seen from Figure 1.5.

The directivity of the antenna is calculated by

$$D(\phi, \varphi) = \frac{r^2 \frac{1}{2} Re[E \times H^*]}{P_{rad}/4\pi} \tag{1.12}$$

where P_{rad} is the radiated power. For a directional antenna, the directivity of the antenna can be estimated by [1]

$$D_0 \simeq \frac{4\pi(180/\pi)^2}{\theta_{1d}\theta_{2d}} = \frac{41253}{\theta_{1d}\theta_{2d}} \tag{1.13}$$

where θ_{1d} and θ_{2d} are the HPBW in two orthogonal planes.

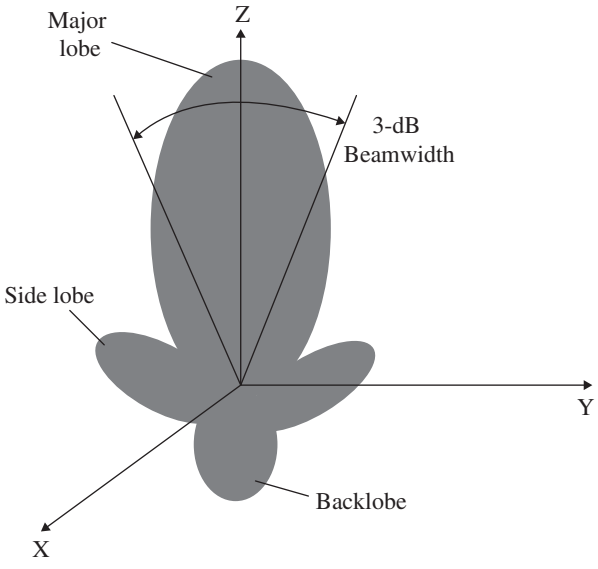

Figure 1.6 Illustration of the HPBW and the lobes of the antenna.

The gain of the antenna (G) is

$$G(\phi, \varphi) = \eta D(\phi, \varphi) \tag{1.14}$$

where η is the radiation efficiency of the antenna. The radiation efficiency describes how much input power is radiated from the antenna and is

$$\eta = \frac{P_{rad}}{P_{in}} \tag{1.15}$$

where P_{in} is the input power and P_{rad} is the radiated power. It is always desirable to have high-efficiency antennas; however, there are always some losses associated with the antenna, such as mismatching, dielectric loss, and conductor loss. The overall efficiency can be written as [1]

$$\eta = \eta_r \eta_c \eta_d \tag{1.16}$$

where η_r is the mismatching efficiency, η_c is the conduction efficiency, and η_d is the dielectric efficiency. The η_c and η_d are related to the material and are frequency dependent. The η_r can be calculated by

$$\eta_r = (1 - |\Gamma|^2) \tag{1.17}$$

When the mismatching efficiency is considered during the calculation, the calculated antenna gain is called the realised gain ($G_{realised}$). This is the overall efficiency of the antenna. Another method to define the antenna efficiency is to use the effective aperture, and the antenna efficiency is defined as the ratio of the effective area aperture to the actual physical size of the antenna

$$\eta = \frac{A_{eff}}{A} \tag{1.18}$$

where A represents the physical aperture size and A_{eff} represents the effective aperture size of the antenna. The A_{eff} can be calculated by

$$A_{eff} = \frac{\lambda^2}{4\pi} G \tag{1.19}$$

1.2.3 Polarisations

The polarisation of an antenna is defined as the polarisation of the wave radiated by the antenna [1]. Depending on the orientation of the electric field, the polarisation of the antenna can be classified as linearly polarised, circularly polarised or elliptically polarised.

Assume a plane wave travelling in the $-z$ direction, which can be written as

$$\vec{E}(z,t) = \vec{x}E_{x0}\cos(\omega t + kz + \phi_x) + \vec{y}E_{y0}\cos(\omega t + kz + \phi_y) \tag{1.20}$$

where E_{x0} and E_{y0} are the maximum magnitudes of the x and y components, respectively. The antenna is linearly polarised if the phase difference between these two components is 180° or

$$\Delta\phi = |\phi_x - \phi_y| = n\pi, n = 0, 1, 2, \ldots \tag{1.21}$$

If the amplitudes of the x and y components are the same while the phase difference $\Delta\phi$ is 90°, the antenna is circularly polarised

$$\Delta\phi = |\phi_x - \phi_y| = n\pi/2, n = 1, 3, 5, \ldots \tag{1.22}$$

$$E_{x0} = E_{y0} \tag{1.23}$$

For a circularly polarised wave, the electric vector at a given point in space traced as a function of time is a circle. The sense of rotation can be determined by observing the direction of the field's rotation as the wave is viewed along the direction of propagation. If the rotation is clockwise, the wave is right-hand circularly polarised (RHCP). If the field rotation is anti-clockwise, the wave is left-hand circularly polarised (LHCP).

If the amplitudes of the x and y components are not equal but the phase difference $\Delta\phi$ is 90°, then the antenna is elliptically polarised

$$\Delta\phi = |\phi_x - \phi_y| = n\pi/2, n = 1, 3, 5, \ldots \tag{1.24}$$

$$E_{x0} \neq E_{y0} \tag{1.25}$$

For the elliptical polarisation, the electric vector traced at a given position is a tilted ellipse, as shown in Figure 1.7. In practice, it is impossible to obtain a pure circularly polarised antenna within the entire bandwidth of the antenna. Thus, the term axial ratio (AR) is defined to describe how circular the radiated wave is. It is defined as the ratio of the major axis to the minor axis of the ellipse [1]

$$AR = \frac{OA}{OB} \tag{1.26}$$

where OA represents the major axis and OB represents the minor axis of the ellipse. These can be calculated by using the following equations

$$OA = \left[\frac{1}{2}(E_{x0}^2 + E_{y0}^2) + [E_{x0}^4 + E_{y0}^4 + 2E_{x0}^2E_{y0}^2\cos(2\Delta\phi)]^{1/2}\right]^{1/2} \tag{1.27}$$

$$OB = \left[\frac{1}{2}(E_{x0}^2 + E_{y0}^2) - [E_{x0}^4 + E_{y0}^4 + 2E_{x0}^2E_{y0}^2\cos(2\Delta\phi)]^{1/2}\right]^{1/2} \tag{1.28}$$

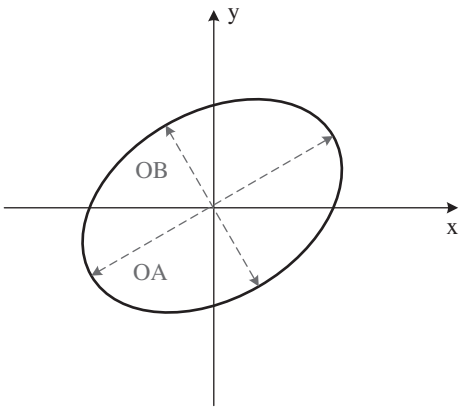

Figure 1.7 Tilted ellipse of elliptical polarisation.

The tilt angle of the ellipse relative to the y axis is

$$\tau = \frac{\pi}{2} - \frac{1}{2}\tan^{-1}\left[\frac{2E_{x0}E_{y0}}{E_{x0}^2 - E_{y0}^2}\cos(\Delta\phi)\right] \tag{1.29}$$

AR is an important parameter of a circularly polarised antenna. Normally it is required that the AR of a circularly polarised antenna at the frequency band of interest is below 3 dB. In some applications, such as satellite communications, the requirement for the AR is more rigorous. For a circularly polarised antenna, it is important to check both the impedance and AR bandwidth, as they do not necessary overlap in the same frequency range. As an example, Figure 1.8a shows the impedance and AR bandwidth of a circularly polarised patch antenna. The AR is taken at the angle $\theta = 0^\circ$ where the maximum gain of the patch is. This patch is a probe-fed square patch and has resonance at 7.9 GHz. The patch is corner truncated in order to obtain circular polarisation. Figure 1.8b shows the layout of this circularly polarised patch. The AR minimum is at 7.5 GHz and the AR ($AR < 3$) bandwidth partially overlaps with the impedance bandwidth of the patch.

Besides the bandwidth, another important parameter for a circularly polarised antenna is the AR beamwidth. The AR beamwidth describes the coverage region where the radiated waves from the antenna are circularly polarised. Figure 1.9 shows the simulated radiation pattern of the circularly polarised patch at its resonance in the $\phi = 0^\circ$ plane. As shown, the dominant polarisation of this patch is RHCP and the 3 dB beamwidth of the patch is 80° (from −40° to +40°). The 3 dB AR beamwidth corresponds to the angle range where the LHCP is 15 dB lower than RHCP, which is from −31° to +85°. Thus, the overlapped HPBW and AR beamwidth is from −31° to +40°.

1.3 Antenna Array Fundamentals

An antenna array consists of multiple antenna elements positioned within an aperture. The total radiation pattern of an array antenna is the vector addition of the field radiated by each radiating element, and it can be expressed as the product of the array factor (AF) times the radiation pattern of the isolated radiating element. Each array element is excited by the input RF signal with certain amplitude and phase. By controlling the

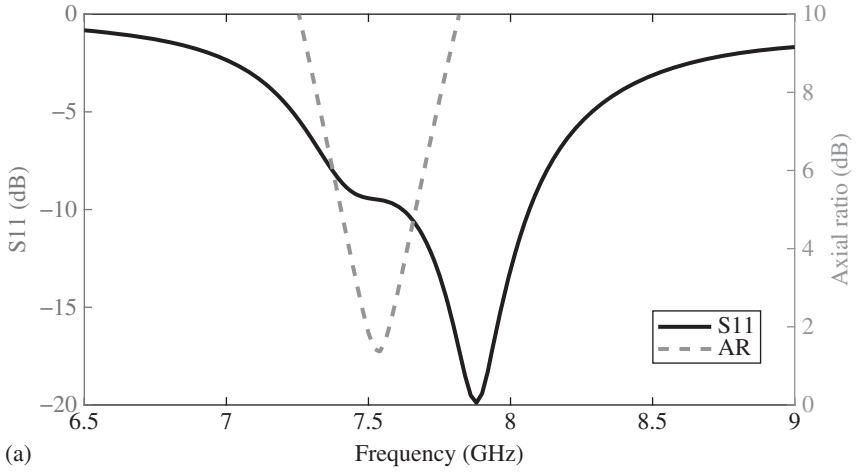

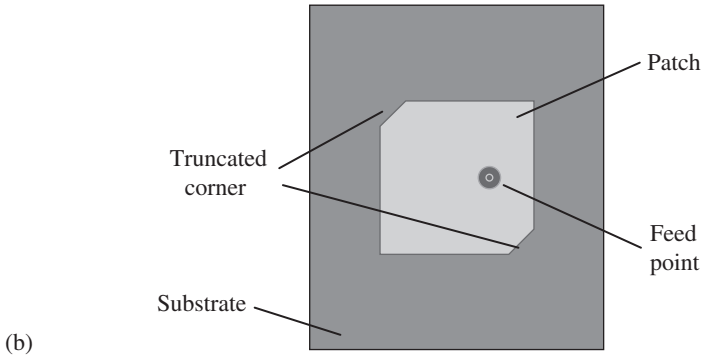

Figure 1.8 (a) The return loss and AR of a patch antenna. (b) The layout of the corner truncated square patch.

excitations of the array antenna, the beams of the array antenna can be formed to provide constructive interference to the desired direction and form nulls at undesired directions.

The array antenna is a critical component of the smart antenna. It determines the beam-steering performance (e.g. the largest beam scanning angle), directivity, and radiation efficiency of the antenna system. The BFN and the microwave circuit determine the beam-steering or beam-switching capability of the array antenna. The antenna array can be either a linear array or a planar array. The linear array is an array of antennas placed along one axis, as shown in Figure 1.10. A number of identical elements are spaced by a distance d and excited with phase difference β. Assuming that these elements are excited by identical amplitudes, the array factor can be derived as [1]

$$AF = \sum_{n=1}^{N} e^{j(n-1)\psi} \tag{1.30}$$

where $\psi = kd\cos\theta + \beta$ and θ is the scan angle of the array antenna.

Besides the linear array configuration, antenna elements can also be placed along a rectangular grid to form a planar array, as shown in Figure 1.11. Planar arrays are more flexible in beamforming and, ideally, the main beam can be steered to any desired

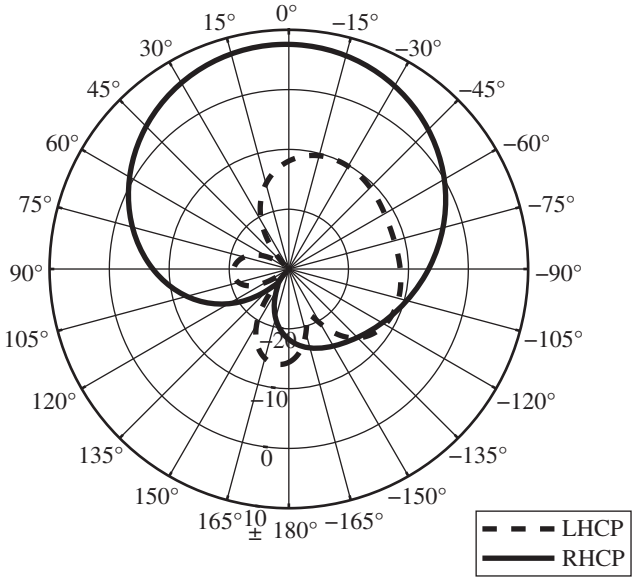

Figure 1.9 The simulated radiation pattern of the circularly polarised patch at its resonance in the $\phi = 0^\circ$ plane.

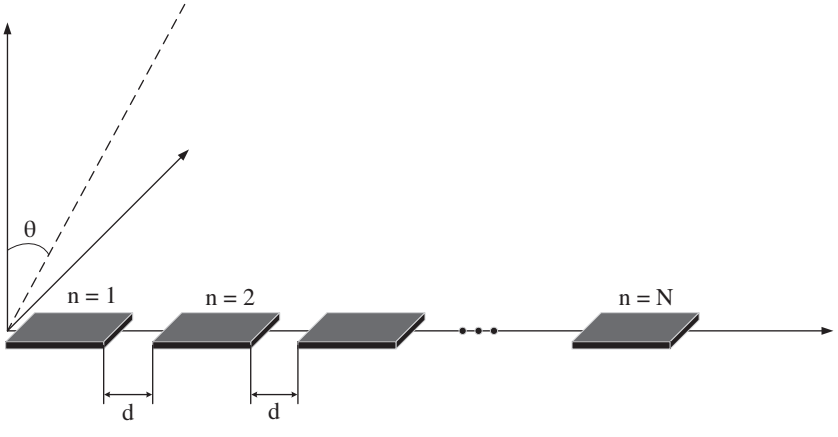

Figure 1.10 Linear array configuration.

direction (θ, ϕ). Thus, in general, the planar array is preferred for the design of smart antennas so it can benefit from the advanced BFN and signal processing algorithm. The array factor of the planar array can be written as [1]

$$AF = S_{xm} S_{yn} \tag{1.31}$$

where

$$S_{xm} = \sum_{m=1}^{M} e^{j(m-1)(kd_x \sin\theta \cos\phi + \beta_x)} \tag{1.32}$$

$$S_{yn} = \sum_{n=1}^{N} e^{j(n-1)(kd_y \sin\theta \sin\phi + \beta_y)} \tag{1.33}$$

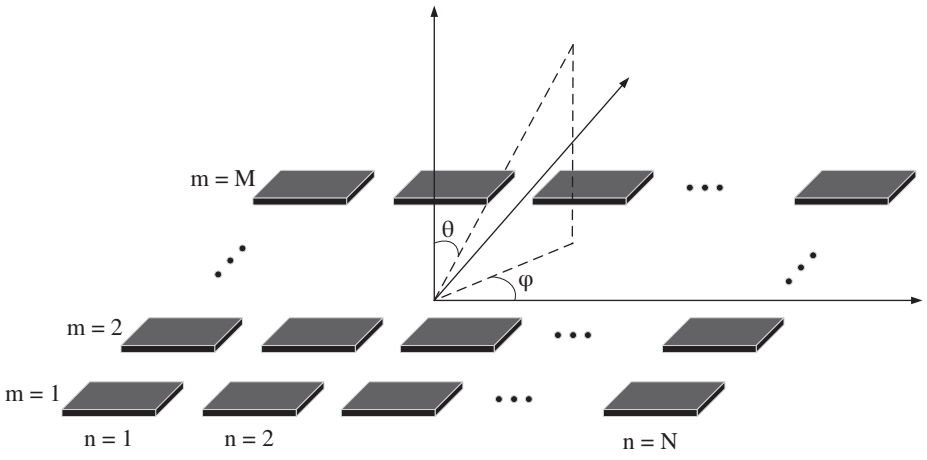

Figure 1.11 Planar array configuration.

d_x and d_y are the distances between the elements in the x and y axes, and β_x and β_y are the phase differences between the elements in the x and y axes, respectively.

1.3.1 Array Performance Analysis

The performance of the array is dependent on the radiation characteristics of the antenna element. There are also other factors that can affect the performance of the array antenna. For example, due to mutual coupling between adjacent elements, the input impedance and radiation pattern of the antenna elements are different from the case where the antenna radiates alone in free space. Therefore, it is a necessary step to analyse the array performance and optimise the array unit cell.

1.3.2 Active Reflection Coefficient and Mutual Coupling

When the array elements are excited, the voltages on each array element are expressed as [4]

$$V_m = \sum Z_{mn} I_n \tag{1.34}$$

where Z_{mn} is the impedance matrix of the whole array. When $m = n$, this represents the self impedance of element n and when $m \neq n$, this represents the mutual impedance between element m and n. I_n represents the amplitude of the current on the element n and V_m represents the applied voltage on the element m. If there is no coupling between the array element m and n, Z_{mn} equals zero and the mutual impedance matrix $[Z_{mn}]$ is diagonal. In general, the mutual coupling between array elements should be minimised in order to reduce the effect of the mutual impedance variations when the array scans [5].

To demonstrate the mutual coupling between the adjacent elements, Figure 1.12 shows the simulated E-field of a two-element array where only one of the antenna elements is excited while the other one is terminated by a matched load. As shown, the radiated field of the antenna is electromagnetically coupled to the other element, which

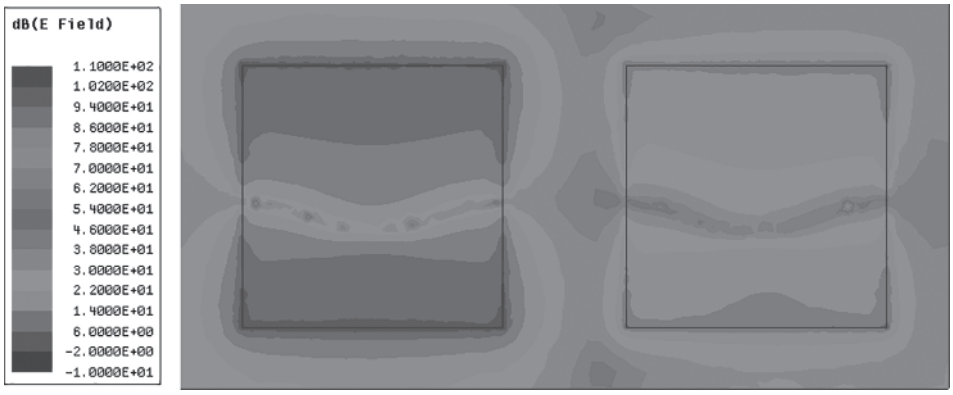

Figure 1.12 The mutual coupling in a two-element array antenna.

has an effect on the input impedance of the element. When there is a large number of elements presented, the mutual couplings are more complicated. One effective way to analyse and predict the radiation performance of the array element is to use the Floquet analysis [6].

In the Floquet analysis, superposition of Floquet modal functions is used to represent an array antenna of infinite size. This method is based on the fact that an infinite array antenna is equivalent to an array of infinite source functions. By performing Fourier transform and using the periodic function, Floquet series and Floquet sources are derived. Although the array antenna has a finite size, the analysis of an infinite array is still useful because the antenna elements in the central region of an electrically large array show similar radiation characteristics to the element in an infinite array after taking consideration of the mutual coupling effects. Moreover, it was shown in [6] that the performance of a finite array can be determined accurately by utilising the results derived in an infinite array. Floquet analysis can be performed in electromagnetic (EM) simulations by designing an array unit cell and assigning it periodic boundary conditions. This provides a good estimation of the input impedance matching, active reflection coefficient and scanning loss of the array antenna without using large computation resources. Figure 1.13 shows the simulated reflection coefficient of an array unit cell at different scan angles. The array unit cell is a square patch resonating at 30 GHz that is simulated using the Floqut port and periodic boundary conditions in a three-dimensional EM simulator. As shown in Figure 1.13, its reflection coefficient changes with different scan angles. This is due to the variation of the mutual couplings with different scan angle, which affects the input impedance of the array element.

Figure 1.14a shows the configuration of a 3×3 array using the square patch as the radiating element. Figure 1.14b compares the simulated active reflection coefficient of the central antenna element with the case when it radiates as an isolated element. The active reflection coefficient is obtained by activating all the nine antennas, while in the other case the reflection coefficient is obtained by only activating the central element and terminating the other elements by 50 Ω loads. As shown, the resonance of the patch shifts to a higher frequency when all the patches are active. Thus, some re-tunings, for example resizing the width of the patch, are required in order to shift the resonance back to the desired frequency.

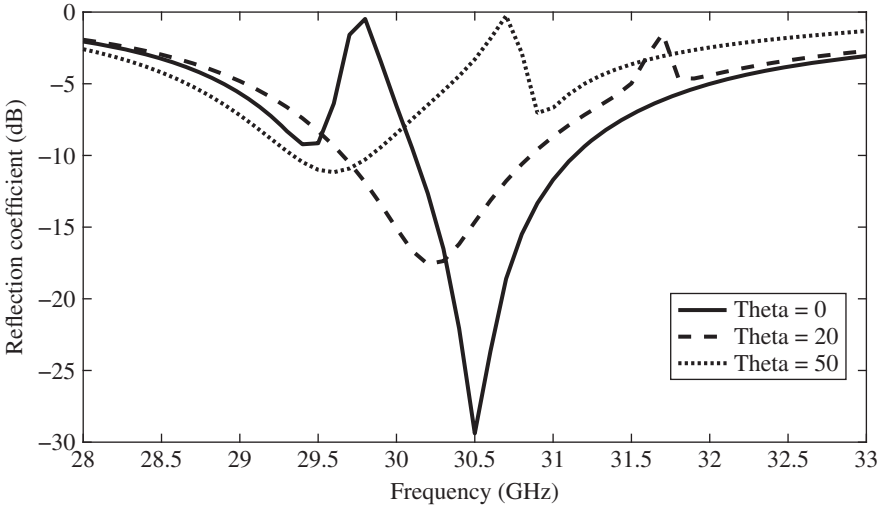

Figure 1.13 Simulated reflection coefficient of an array unit cell with different scan angles.

1.3.3 Directivity and Beamwidth

The directivity (D) of the array antenna is decided by the number of radiating elements when the distance between each array element is fixed [4]

$$D = \frac{4\pi A}{\lambda^2}\varepsilon_A \cos\theta \tag{1.35}$$

where A is the size of the radiating aperture and ε_A is the aperture efficiency of the array. If the beam has a symmetrical pattern in both the E- and H-planes, the 3 dB beamwidth of the array antenna in radians with uniform illumination taper can be estimated by

$$\theta_{3dB} = \sqrt{\frac{4\pi 0.866^2}{D}} \tag{1.36}$$

With the phase and amplitude errors, there would be pointing error, increased sidelobe level and directivity decrease. When phase and amplitude errors present, the directivity of an array antenna and the variance of the beam pointing deviation can be estimated by [4]

$$\frac{D}{D_0} = \frac{P}{1+\overline{\sigma}^2+\overline{\phi}^2} \tag{1.37}$$

$$\overline{\Delta}^2 = \overline{\phi}^2 \frac{\sum I_i^2 x_i^2}{\left(\sum I_i x_i^2\right)^2} \tag{1.38}$$

where D is the directivity of the array with errors, D_0 is the directivity of the array without any phase/amplitude errors, P is the probability that the error happens, ϕ is the phase error, σ is the amplitude error, $\overline{\Delta}$ is the variance of beam pointing deviation, I_i is the amplitude of the ith element excitation, and x_i is the element position divided by element spacing d. Due to the existence of these errors, a smart antenna with a BFN is required to perform calibrations before it is equipped with the communication system.

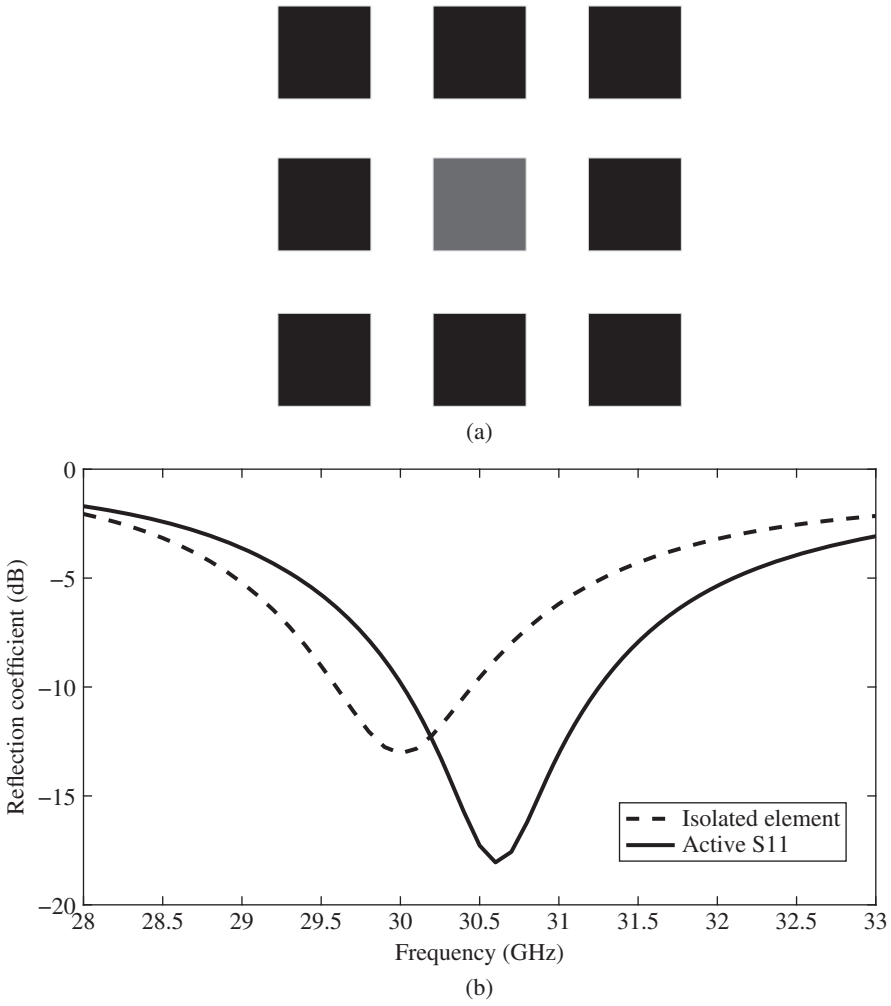

Figure 1.14 (a) Layout of a 3 × 3 array antenna. (b) Comparison between the active and isolated reflection coefficients of the array antenna element.

1.3.4 Grating Lobe

The additional main beam is observed when the spacing between the array elements is large because larger spacing allows the radiated waves from each element to add in phase at other angles besides the main beam of the array [7]. This is called the grating lobe.

The maximum scan angle of a two-dimensional array using a rectangular grid without any grating lobes is calculated by [6]

$$p = \frac{\lambda_0}{1 + \sin\theta_{max}} \tag{1.39}$$

where p is the period of the elements, λ_0 is the free space wavelength and θ_{max} is the maximum scan angle of the array antenna without any grating lobes. Generally

speaking, in order to avoid the grating lobe, the distance between the elements is kept as a half-wavelength.

Given the same grating lobe free area, an array antenna with hexagonal lattice requires 0.866 as many elements as the array antenna with a rectangular lattice [7]. Thus, the distance between the elements can be increased by 1.15 times and the number of elements can be reduced by 15%.

1.3.5 Scan Blindness

The scan blindness of an array is caused by the cancellation of the dominant mode by the higher modes of the radiating element [7]. Scan blindness is also related to a true surface wave supported by the antenna structure [4]. The blind angle of the array can be determined by using the Floquet modal functions. The transverse wavenumbers of the Floquet mode are given by [6]

$$k_{xij} = k_{x0} + \frac{2i\pi}{a} \tag{1.40}$$

$$k_{yij} = k_{y0} - \frac{2i\pi}{a\tan\gamma} + \frac{2j\pi}{b} \tag{1.41}$$

where i and j are the mode numbers for the Floquet mode, and a, b and γ are related to the configuration of the array (array lattice) and are indicated in Figure 1.15. The wavenumbers k_{x0} and k_{y0} are

$$k_{x0} = k_0 \sin\theta\cos\phi \tag{1.42}$$

$$k_{y0} = k_0 \sin\theta\sin\phi \tag{1.43}$$

where θ and ϕ are the intended scan angles of the array. The transverse wavenumbers of the surface wave are given by [6]

$$k_{xs} = k_{\rho s}\cos\alpha + \frac{2m\pi}{a} \tag{1.44}$$

$$k_{ys} = k_{\rho s}\sin\alpha + \frac{2n\pi}{b} \tag{1.45}$$

where α is the propagation angle with the x axis of the surface wave. The $k_{\rho s}$ is estimated by the following expression when the antenna elements are printed on a relatively thin substrate [8]

$$k_{\rho s} \approx k_0[1 + 0.5(k_0 h(1 - \frac{1}{\varepsilon_r}))^2] \tag{1.46}$$

Scan blindness occurs when the wavenumber of the surface wave matches the wavenumber of the Floquet mode. This means that there is a strong coupling between the surface wave and the Floquet mode. Since a rectangular grid is employed in this study and it is known that (0,0) is the dominant Floquet mode, the following equations are derived from [6]

$$k_{\rho s}\cos\alpha + \frac{2m\pi}{a} = k_0 \sin\theta_{blind}\cos\phi \tag{1.47}$$

$$k_{\rho s}\cos\alpha + \frac{2n\pi}{b} = k_0 \sin\theta_{blind}\sin\phi \tag{1.48}$$

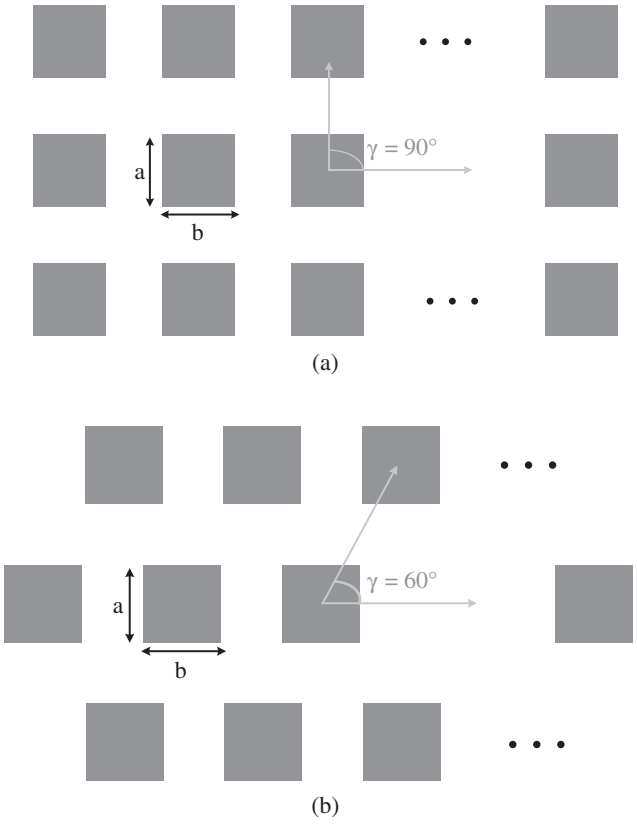

Figure 1.15 Illustration of the parameters used in Floquet mode analysis: (a) rectangular lattice and (b) hexagonal lattice.

where θ_{blind} is the scan blindness angle, and m, n is the mode number. At the scan blindness angle, all of the power incident on the array is trapped in the non-radiating surface wave, which results in total reflection ($|S11| \approx 0\ dB$) [9]. As shown in Figure 1.13, total reflection takes place at certain frequencies when the array scans, which means that scan blindness would occur at these frequencies and scan angles.

1.4 Smart Antenna Architecture and Hardware Implementation

A smart antenna consists of an array antenna and a signal processing unit. The signal processing unit uses some advanced algorithms to identify the DOA of the signal and calculate beamforming vectors, which steer the beam of the array antenna to the desired direction and suppress the lobes at unwanted angles. Figure 1.16 shows the generic system configuration of a smart antenna.

Smart antennas can be categorised into two main types: beam-switching antenna systems and adaptive array antenna systems. The beam-switching smart antenna has a BFN

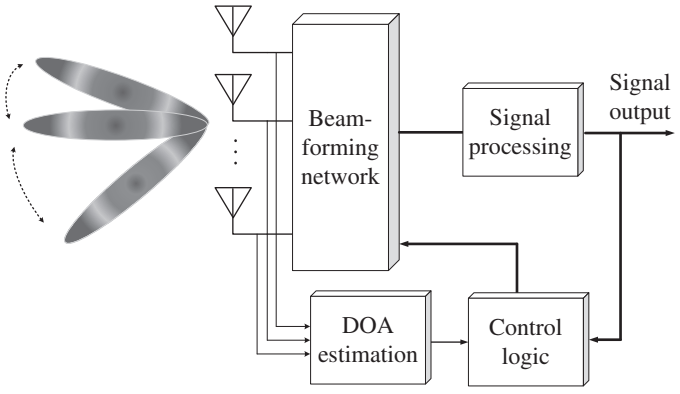

Figure 1.16 The generic system configuration of a smart antenna.

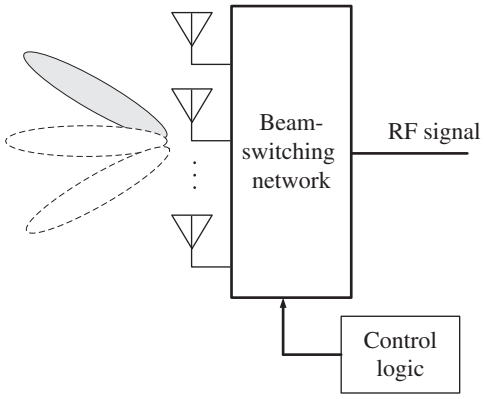

Figure 1.17 A typical architecture for a beam-switching antenna system.

that provides the fixed phase shift to form shaped beams in pre-defined directions. Figure 1.17 shows a typical architecture for a beam-switching smart antenna. It consists of an antenna array, a beamforming feed network and a control unit for beam selection. The antenna array can be either a linear or a planar array, depending on the requirements of the targeted applications. The beamforming feed network is a critical component because it determines the number of available beams that can be switched. The most common techniques for designing a beam-switching network include the use of the Butler matrix, introducing microwave switches such as PIN diodes or RF micro-electromechanical system (MEMS) switches on the feed network [10–12]. Since they do not need to employ any phase shifters and their control circuits are relatively simple, beam-switching smart antennas provide a low-cost and low-power consumption solution if continuous beam-steering is not required. The main disadvantage for the beam-switching smart antenna is that it can only provide a limited number of beams. For example, the parasitic array antenna only has one driven element surrounded by several parasitic elements. Beam-switching is obtained by controlling the reactive loads of the parasitic elements. The number of achievable beams is limited and is determined by the number of parasitic elements as well as the adjustable range of the reactive loads.

Adaptive smart antennas are able to continuously steer the beam to the desired directions and shape the beam to maximise the link budget with sophisticated

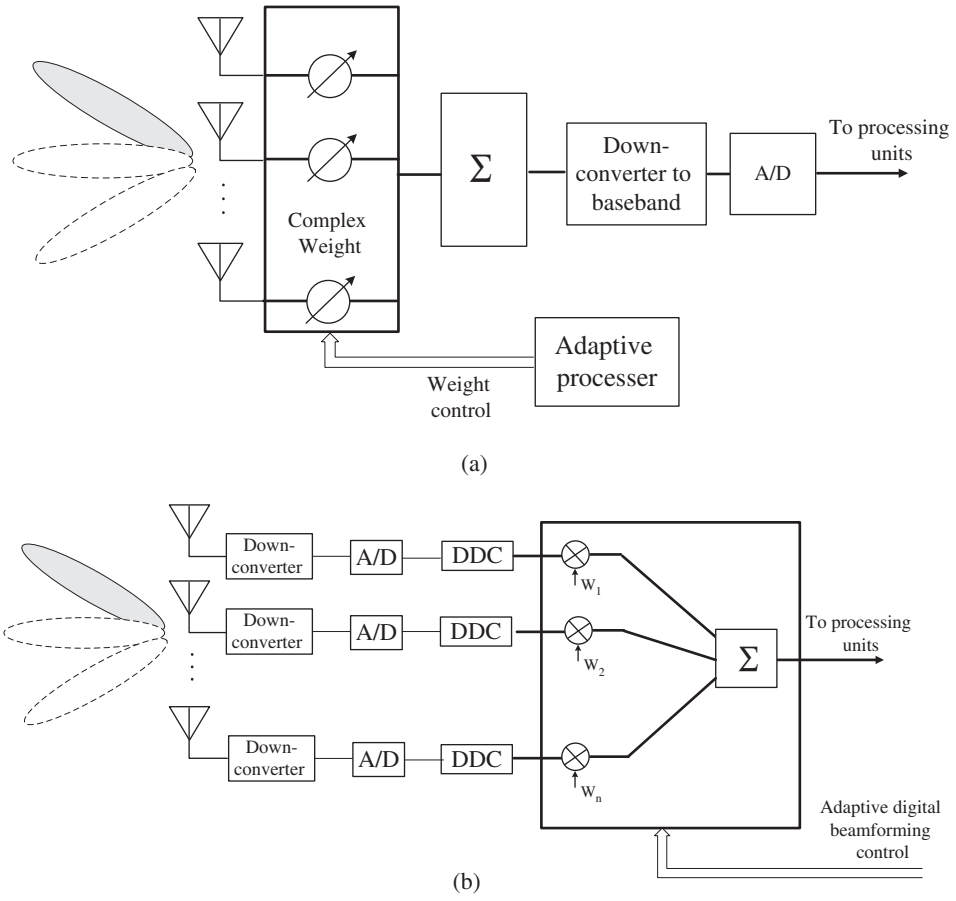

Figure 1.18 The generic system architecture of: (a) the smart array antenna using analogue beamforming and (b) digital beamforming.

signal processing algorithms. The beamforming of the adaptive array antennas can be achieved by two approaches: analogue or digital. Figure 1.18 shows the generic system architecture of the smart array using analogue beamforming (ABF) and digital beamforming (DBF).

ABF requires the use of a large number of phase shifters and attenuators to provide complex weights to the array elements. The summed signals need to be down-converted to baseband signals then pass to the analogue/digital (A/D) converter before being sent to the signal processing unit. Instead of using a large number of microwave phase shifters, which are expensive and lossy, DBF uses an A/D converter and a digital down-converter (DDC) on each array element and then the beamforming can be realised digitally. However, DBF requires a large number of A/D converters, which have high power consumption and need real-time signal processing. To realise adaptive beamforming, there are several well-defined algorithms available, such as the LMS algorithm, the recursive least squares algorithm and the CMA. Some low-cost beamforming algorithms are summarised in Chapter 2 and readers can refer to this

Table 1.1 Comparison of the beam-switching and adaptive arrays.

	Beam-switching array	Adaptive array
Cover range	Larger than traditional antenna system	Larger than beam-switching antenna system
Signal processing	Basic	Advanced
System complexity	Low	High
Beamforming	Limited	Advanced
Power consumption	Low/medium	High
Interference rejection capability	Poor	Good
Cost	Low	High

chapter for more details. Table 1.1 compares the beam-switching array and adaptive array in terms of the performance, system complexity and cost.

1.4.1 ADC and DAC

The analogue-to-digital converter (ADC) converts an analogue signal into a digital signal while the digital-to-analogue converter (DAC) converts a digital signal into an analogue signal. The ADC is used in the receiving system and the DAC is used at the transmitter. Resolution is one of the key parameters for the ADC, as it determines the quantisation error. For example, an ADC with a resolution of 6 bits can encode an analogue input to one in 64 different levels ($2^6 = 64$). Ideally, the quantisation error for the ADC should be as small as possible. However, a higher resolution converter normally has a higher cost.

Another important parameter of the ADC is the sampling rate. Based on Nyquist sampling theorem, a signal should be sampled at a rate greater than twice its maximum frequency component. For a wideband antenna system, this means that it needs a very high sampling rate. A high sampling rate ADC needs to consume more power and the cost is high. For a low-cost system, the undersampling technique can be used. The advantages of undersampling include low power consumption, low cost, easy capturing of ADC data, and easy interface to field-programmable gate arrays (FPGAs) (because of its lower speeds) [13].

1.4.2 Digital Down-Converter (DDC)

The DDC converts the digitised signal (e.g. the output of the ADC) to a lower frequency signal at a lower sampling rate. The DDC is normally used in the digital beamforming system, where the received signal from each of the antenna elements is down-converted and converted to the digital signals.

1.4.3 Digital Signal Processor

A digital signal processor (DSP) is a microprocessor that processes the digitalised signals and performs the mathematical manipulation. The DSP is important hardware for the

smart antenna because it performs signal processing and beamforming. A DSP contains the program memory, data memory, compute engine, and input/output [14]. The program memory stores the programs that can be used to perform the signal processing, such as the beamforming algorithms, while the data memory saves the information to be processed. The compute engine processes the digital signal using the program saved in the program memory and the data stored in the data memory. For a smart antenna with a sophisticated signal processing algorithm, the DSP needs to have large computation resource and consume more power. A typical example is the digital BFN.

1.4.4 Field-programmable Gate Array

The development of the FPGA provides an alternative way to design the BFN of smart antennas [15, 16]. FPGAs contain an array of programmable logic blocks and can be reconfigured for different applications. They have embedded processors, which provide options for implementing various adaptive signal processing algorithms such as DOA estimation, MUltiple SIgnal Classification (MUSIC), and the LMS algorithm. It is also possible to have a PFGA board with built-in A/D converter and other modules as well. Figure 1.19 is a diagram of a smart antenna using FPGA.

To reduce the cost, the price of a high-end PFGA and related modules puts pressure on the development of low-cost smart antennas. Using some external modules instead of embedding the modules (e.g. external ADC) on the FPGA reduces the cost of the system. A low-cost hardware implementation of a smart antenna based on FPGA was reported in [17]. The beamforming algorithm was implemented on a low-end FPGA and the adaptive beamforming was realised by using the CMA.

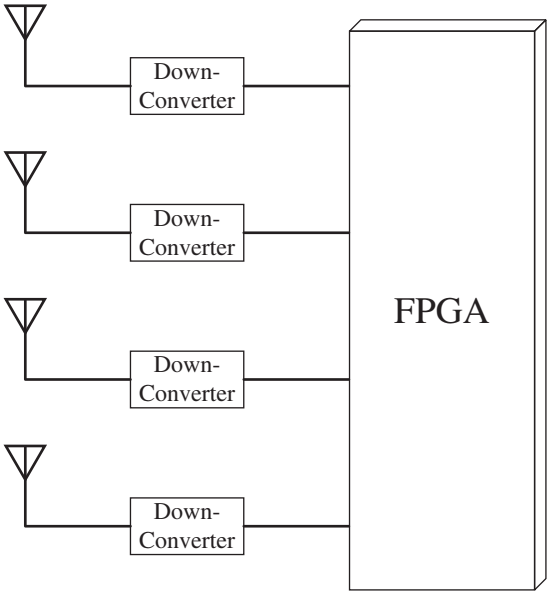

Figure 1.19 A block diagram of a smart antenna using FPGA.

1.5 Overview of the Book

The book contains seven chapters. Chapter 1 presents a brief discussion on antenna and array antenna fundamentals, as well as smart antenna configurations. The aim of the chapter is to provide readers with some basic concepts and fundamental theories of the RF part of smart antennas.

Chapter 2 discusses the basic principles of beamforming and introduces some representative beamforming methods and algorithms for smart antennas. A review of the particular area of low-cost adaptive beamforming is also presented in this chapter, including hybrid beamforming and robust adaptive beamforming. The objective of the chapter is to provide readers with some basics of beamforming algorithms and their applications in wireless commutations. A list of references is provided in the end of this chapter and interested readers can refer to these references for more details.

Chapter 3 presents low-cost smart antenna design using the electronically steerable parasitic array radiator (ESPAR). ESPAR is an attractive solution to the design of low-cost smart antenna because it has only one RF transceiver and the electronic beam scanning of the antenna system can be achieved without using any phase shifters. This chapter introduces various designs of the ESPAR using different types of antenna elements, such as monopole, microstrip slot antenna, and patch. Varactors or PIN diodes can be employed to load the parasitic elements of ESPAR, and many examples are discussed in this chapter. The link quality test is performed to validate channel improvement using the ESPAR.

Chapter 4 presents the design of beam-switching and beam-steering antenna using the active frequency selective surface (FSS). The FSS is a periodic structure that shows space filtering characteristics, for example bandpass or bandstop. By incorporating RF PIN diodes or varactors in the FSS, the characteristics of the FSS can be controlled. In this chapter, the fundamental theories of the FSS are presented first, then different approaches to realise a low-cost beam-switching and beam-steering antenna using active FSS are discussed with design examples, including some practical techniques to design the bias circuit to control the FSS.

In Chapter 5 the design of beam-scanning and beam-switching reflectarrays and transmitarrays is discussed. Both types of antennas are space-fed and they can operate without the use of the feed network. By placing the feeds in the focal arc, multibeam or beam switching can be obtained. They are suitable for the applications where beam switching, high directivity, and low cost are required. This chapter presents the fundamental theories and operation principles of the reflectarrays and transmitarrays with design examples. Some discussions on circularly polarised design are also included in this chapter.

MIMO antenna uses multiple antennas at the transmitter and receiver to increase channel throughput by taking advantage of the space diversity. Chapter 6 presents the MIMO theories and discusses different approaches to design compact low-cost MIMO antennas, such as the use of neutralising lines, decoupling networks, and metamaterials. A case study is given to demonstrate how to improve the isolation between two closely spaced planar inverted-F antennas for smartphones.

Chapter 7 presents some other types of low-cost smart antennas, including dielectric lenses, retrodirective arrays, Fabry–Perot resonant antennas, array-fed reflectors and multibeam antennas based on BFNs. The basic principles and design techniques of

various types of low-cost smart antennas are explained, and many examples of recent developments in each type of smart antennas are discussed. These are useful for readers who need to understand different techniques in low-cost smart antennas in order to choose a specific type of smart antenna for relevant applications.

References

1 C.A. Balanis. *Antenna Theory: Analysis and Design*. John Wiley & Sons Inc., 3rd edition, 2015.

2 W.A. Imbriale, S. Gao, and L. Boccia, editors. *Space Antenna Handbook*. John Wiley & Sons Ltd, 2012.

3 J.D. Kraus and R.J. Marhelfa. *Antenna for all Applications*. McGraw-Hill, 2002.

4 R.J. Mailloux. *Phased Array Antenna Handbook*. Artech House Inc., 2005.

5 P.W. Hannan, D. Lerner, and G. Knittel. Impedance matching a phased-array antenna over wide scan angles by connecting circuits. *IEEE Transactions on Antennas and Propagation*, 13(1):28–34, Jan 1965.

6 A.K. Bhattacharyya. *Phased Array Antennas: Floquet analysis, synthesis, BFNs, and active array systems*. John Wiley & Sons Inc., 2006.

7 R.C. Hansen. *Phased Array Antennas*. John Wiley & Sons Inc., 2009.

8 W.C. Chew, J.A. Kong, and L.C. Shen. Radiation characteristics of a circular microstrip antenna. *Journal of Applied Physics*, 51(7):3907–3915, 1980.

9 D. Pozar and D. Schaubert. Scan blindness in infinite phased arrays of printed dipoles. *IEEE Transactions on Antennas and Propagation*, 32(6):602–610, Jun 1984.

10 W.F. Moulder, W. Khalil, and J.L. Volakis. 60-GHz two-dimensionally scanning array employing wideband planar switched beam network. *IEEE Antennas and Wireless Propagation Letters*, 9:818–821, 2010.

11 S.A. Mitilineos and C.N. Capsalis. A new, low-cost, switched beam and fully adaptive antenna array for 2.4 GHz ISM applications. *IEEE Transactions on Antennas and Propagation*, 55(9):2502–2508, Sept 2007.

12 C.E. Patterson, W.T. Khan, G.E. Ponchak, G.S. May, and J. Papapolymerou. A 60-GHz active receiving switched-beam antenna array with integrated butler matrix and GaAs amplifiers. *IEEE Transactions on Microwave Theory and Techniques*, 60(11):3599–3607, Nov 2012.

13 Texas Instruments. Why oversample when undersampling can do the job? Technical report, 2013.

14 Analog Devices. A beginner's guide to digital signal processing (DSP). Technical report, accessed in March 2018.

15 M. Kim, K. Ichige, and H. Arai. Real-time smart antenna system incorporating FPGA-based fast DOA estimator. In *IEEE 60th Vehicular Technology Conference, 2004. VTC2004-Fall. 2004*, volume 1, pages 160–164 Vol. 1, Sept 2004.

16 H. Arai and K. Ichige. *Hardware Implementation of Smart Antenna Systems for High Speed Wireless Communication*. Proceedings of 2005 URSI General Assembly, No. BC-6, New Delhi, 2005.

17 A. Chinatto, C. Junqueira, and J.M.T. Romano. Low cost smart antenna array hardware implementation. In *2011 SBMO/IEEE MTT-S International Microwave and Optoelectronics Conference (IMOC 2011)*, pages 784–788, Oct 2011.